

# Waves and Turbulence Experiment: Grand Passage, 9-27 June 2018

Anneke ten Doeschate, Richard Cheel and Alex E. Hay  
Department of Oceanography  
Dalhousie University

submitted to the

Offshore Energy Research Association

November 13, 2019

# 1 Introduction

This report briefly summarizes results from a measurement campaign carried out in June 2018 at the southern entrance to Grand Passage, NS. The goals of the experiment were: (a) to investigate wave/current/turbulence interactions using bottom-mounted 5-beam acoustic Doppler current profilers; (b) to incorporate a gimballed ADCP mount in the bottom pods, so that the ADCP would maintain a vertical orientation independent of the orientation of the pod once deployed on the very rough and irregular seabed in the passage. The timing of the experiment was dictated by the 31 May end of the lobster season and the 30 June end date for the award to Dr. ten Doeschate from the Dobbin Atlantic Scholarship Foundation for a one-month visit to Dalhousie from Ireland, which she received in order to gain experience with ADCP operation and data processing.

## 2 Experiment description

Frames for the bottom pods were constructed from solid fiberglass rod, non-magnetic cast steel connecting clamps, and fiberglass grating. Each pod supported a 5-beam acoustic Doppler current profiler, mounted in a gimbal. Plastic sheet was mounted around the frame, to serve as a flow shield (see Fig. 1). Both frames were ballasted with three 50 kg lead feet. An acoustically-activated float-line release system was used for recovery. This release system is described elsewhere (*1*).



Figure 1: Left panel: The Signature500 being deployed, showing the flow shield skirt (white) and the top part of the tower for the float-line recovery system (green). Middle and right panels: the frame during construction, showing the recovery system tower containing the float and recovery line, the flow shield skirt, and the ADCP in its gimbal mount.

The pods were deployed at the locations indicated in Fig. 2 for a period of 18 days. The pod with the Nortek Signature500 5-beam ADCP was located to the south of the channel entrance; the pod with the Signature1000 was inside the entrance. The Signature500 was deployed on 9 June 2018, 1340 h ADT, and recovered on 27 June 2018, 1130 h. The Signature1000 was deployed on 9 June 2018 at

ADCP (kHz)	NLat (deg)	WLon (deg)	Depth (m)	Sampling Rate (Hz)	Cell Size (m)
500	44.254	66.332	20.5	4	0.5
1000	44.260	66.334	15.8	8	0.25

Table 1: ADCP positions and settings

1350 h ADT, and recovered on 27 June 2018 at 1145 h. The velocity data were recorded as single-ping profiles, in beam co-ordinates. The Signature500 recorded continuously; the Signature1000 in 6-minute intervals, switching between normal Broadband (BB) mode and High Resolution (HR) mode at the end of each interval. The latitude/longitude locations the two ADCPs are listed together with other instrument settings in Table 1. The mean orientation of each bottom pod over the course of the deployment is shown in Fig. 2.

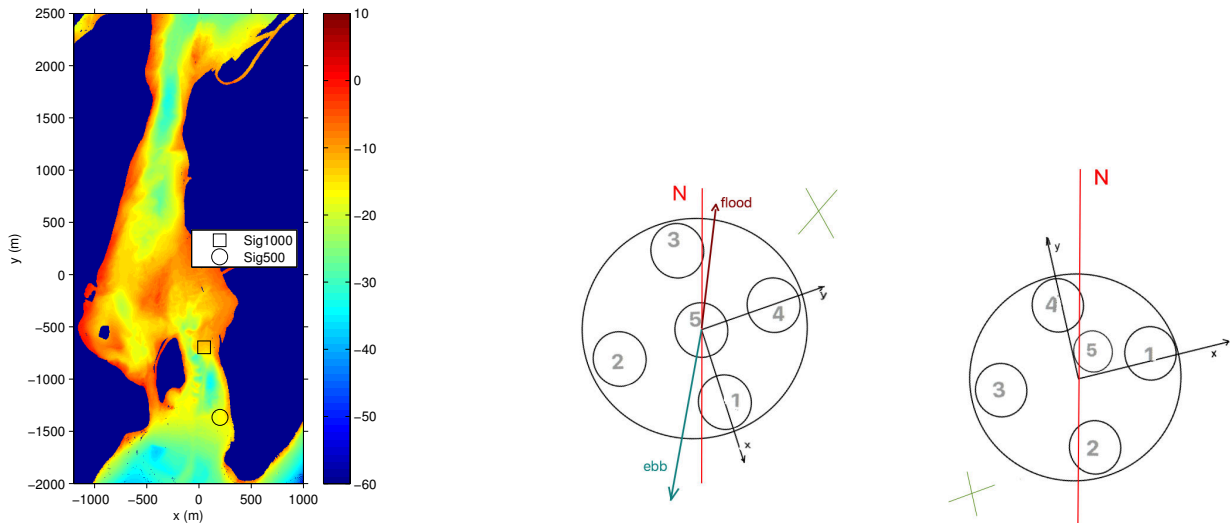


Figure 2: Left: Grand Passage bathymetry, in m. The bottom pod locations are indicated, with Sig500 and Sig1000 denoting the Nortek Signature500 and Signature1000 5-beam ADCPs. Middle and right: mean orientations of the Signature 500 (middle) and Signature 1000 (right) with respect to magnetic north. The  $x$  and  $y$  instrument coordinate axes are indicated. The X indicates the location on the frame of the float line recovery tower (see Fig. 1). Mean flood and ebb directions are indicated by the red and blue arrows.

To accommodate the power requirement for three week's continuous ADCP operation at the desired single-ping data rate (Table 1), external battery cases were required. To implement the gimballed mount, an axially symmetric 2.5 kg lead weight was installed in the ADCP pressure housing in the space normally occupied by the internal battery pack: i.e., at the base of the housing. The purpose of the lead weight was to provide a high righting moment for the ADCP. As the data presented in Figs. 3 and 4 demonstrate, however, neither ADCP maintained a stable vertical orientation over the course of the experiment. Both sets of time series exhibit significant fluctuations about the mean values of

heading, pitch and roll, and the mean pitch and roll values are significantly different from zero. These non-zero mean values indicate that something exerted a net torque on the ADCP housing: i.e., the cable connecting the ADCP to the external power pack case .

The 6-min average headings changed significantly during the course of the experiment. The Signature500 shifted twice, on yd164 and yd170 (Fig. 3b), both times in association with pronounced increases in the variance of the pressure (Fig. 3e). As will be seen, these increased pressure variance levels are associated with wave events. The Signature1000 heading underwent abrupt shifts more often than the Signature500 (Fig. 4), both in association with increased pressure variance (yd164 and 170) and not (yd161). On yd164 and 170, the mean pitch exceeded 30 degrees, indicating that something – kelp perhaps – must have been jammed in the gimbal rings – and broke free afterwards.

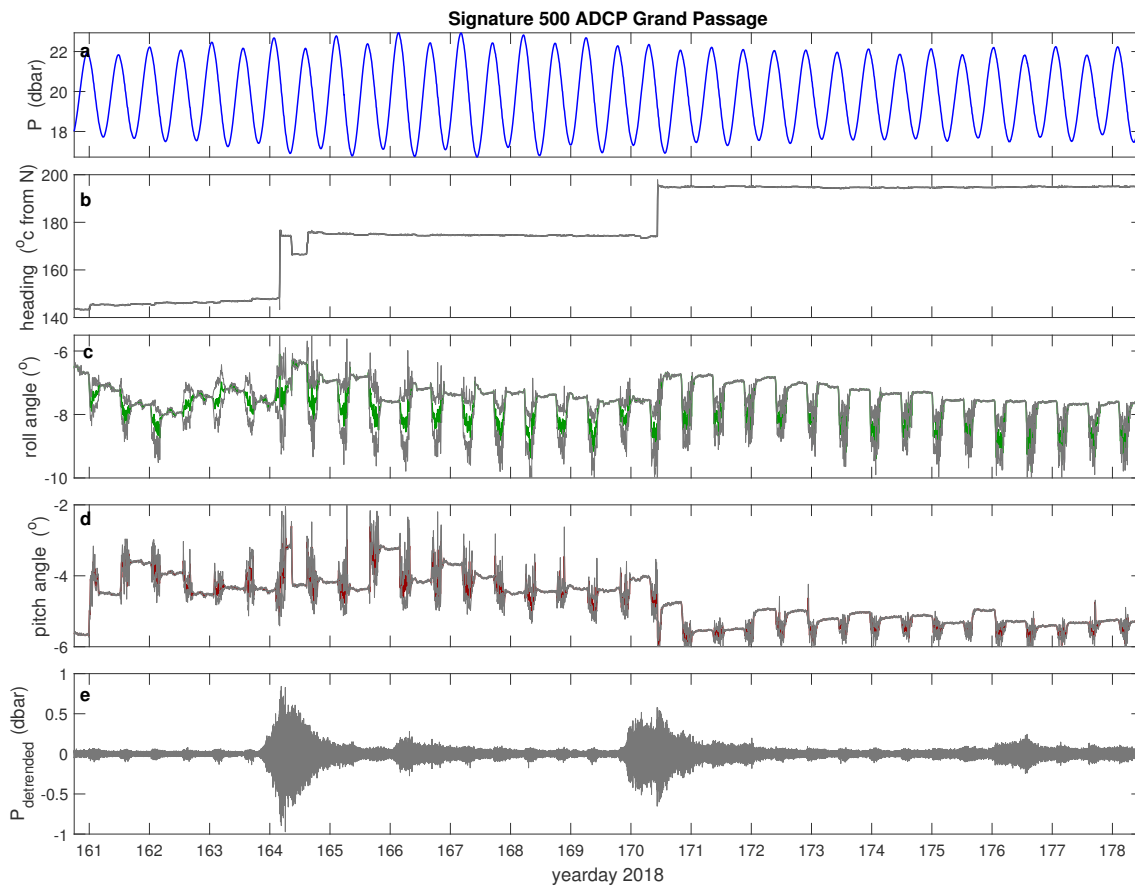


Figure 3: Time series recorded by the Nortek Signature500 ADCP. (a) mean pressure. (b) through (d): mean  $\pm 1$  standard deviation (grey) of compass heading, roll, and pitch, respectively. (e) high-pass filtered pressure, 0.02 Hz cut-off. Time is yearday 2018, UTC.

The pitch and roll time series for both instruments also exhibit variability on tidal time scales. For the Signature500 this variability is manifested as pronounced increases in the pitch and roll standard deviation, during ebb but not flood (Fig. 3c and d). The increased standard deviations are accompanied by ca. 1 degree decrease in mean roll. The pitch and roll for the Signature1000 also exhibit tidal

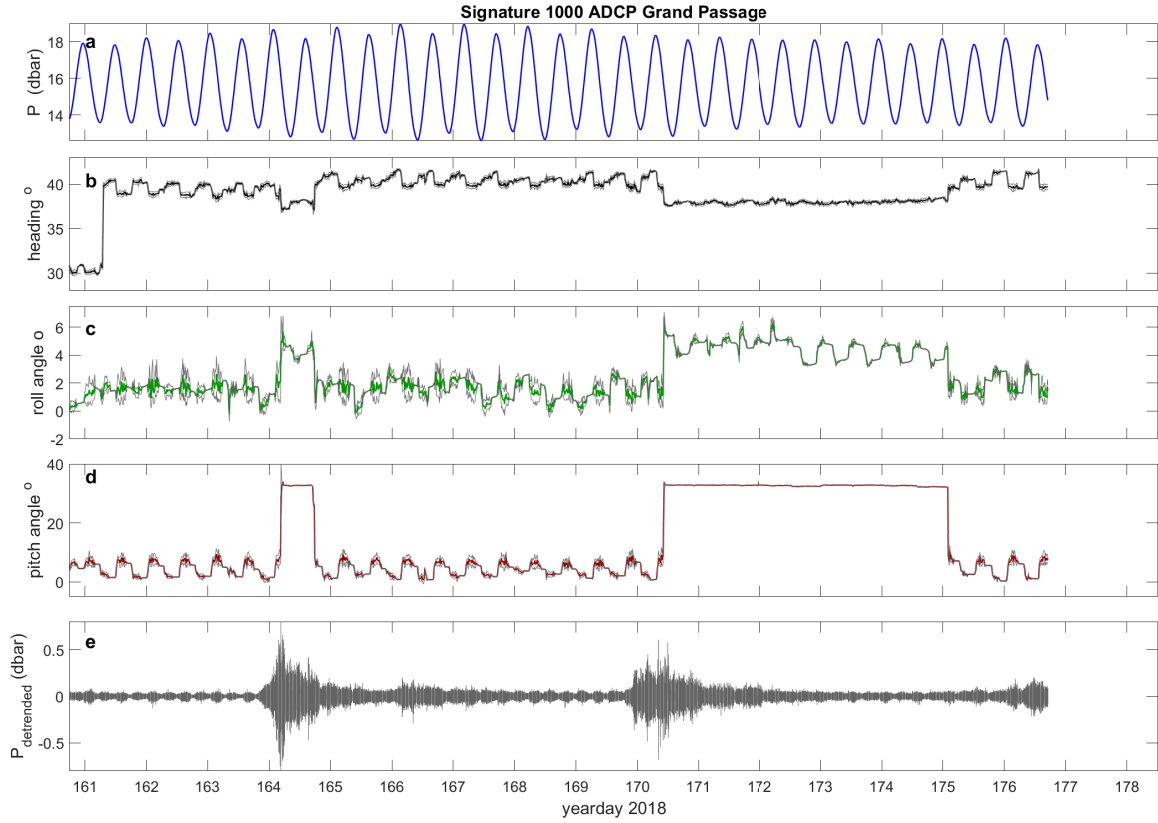


Figure 4: As in Figure 3 but for the Signature1000.

variability in the pitch and roll means and standard deviations, but during both ebb and flood. The association of increased pitch and roll variability on the rising and falling tide points indicates that this variability occurs during times of higher flow speed. The increased variability in the Signature500 data during ebb but not flood is due – as will be seen – to the flood speeds being much lower than ebb speeds at this location: i.e. outside the southern entrance to Grand Passage (Fig. 2).

### 3 Data Processing

#### 3.1 Currents

The along-beam velocities,  $b_{1,2,..,5}$ , recorded by the ADCPs were transformed to instrument coordinate velocities  $u, v, w$  using

$$u = \frac{b_1 - b_3}{2 \sin \theta}, \quad v = \frac{b_4 - b_2}{2 \sin \theta}, \quad w_{13} = \frac{b_1 + b_3}{2 \cos \theta}, \quad w_{24} = \frac{b_2 + b_4}{2 \cos \theta}, \quad w_5 = b_5. \quad (1)$$

where  $\theta$  is the beam angle relative to the instrument axis of symmetry,  $u$  and  $v$  are the horizontal

velocity components along the  $x$  and  $y$  directions (Fig. 2), and  $w$  is the vertical component. The three independent estimates of  $w$  in the above equations provide a quality control check on the measurements.

The  $u, v, w$  velocities were transformed to Earth coordinate velocities,  $U_E, V_N, W$ , representing positive East, North and Up respectively, using the instrument orientation data via the heading rotation matrix,  $H$ , and the pitch-and-roll rotation matrix,  $T$ :

$$H = \begin{bmatrix} \cos \phi_1 & \sin \phi_1 & 0 \\ -\sin \phi_1 & \cos \phi_1 & 0 \\ 0 & 0 & 1 \end{bmatrix} \quad (2)$$

$$T = \begin{bmatrix} \cos \phi_3 & -\sin \phi_3 \sin \phi_2 & -\cos \phi_2 \sin \phi_3 \\ 0 & \cos \phi_2 & -\sin \phi_2 \\ \sin \phi_3 & \sin \phi_2 \cos \phi_3 & \cos \phi_3 \cos \phi_2 \end{bmatrix} \quad (3)$$

The product operator  $H \times T$  performs the transformation from  $u, v, w$  to  $U_E, V_N, W$ . Average velocities, as well as correlations and backscatter amplitudes, were computed for each 6-min burst of the Signature1000, and 6-min segments of the continuous Signature500 record.

### 3.2 Wave height

Pressure spectra were computed from linearly detrended 6-minute records using 512-point, Hamming-windowed segments with 50% overlap. The noise level in each spectrum above the wind wave band (0.05 to 0.3 Hz) was determined by calculating the mean spectral density over the frequency range  $f = 0.35$  Hz to the Nyquist frequency,  $f_{Ny}$ . These noise levels were subtracted from the pressure spectra prior to computing wave height.

The noise-corrected pressure spectra were transformed to surface displacement spectra using linear wave theory (2). Pressure fluctuations,  $p'$ , at depth  $z$  are related to surface elevation  $\eta$  by:

$$p' = \rho g \frac{\cosh k(z + H)}{\cosh kH} \eta. \quad (4)$$

where  $H$  is the mean water depth and  $k = 2\pi/\lambda$  is the wavenumber, with  $\lambda$  being the wavelength. The pressure spectrum  $S_{pp}$  was transformed to a surface elevation spectrum  $S_{\eta\eta}$  over the wind wave band using:

$$S_{\eta\eta}(f) = S_{pp}(f)/M^2, \quad (5)$$

with

$$M(f) = \frac{\cosh k(z + H)}{\cosh kH}. \quad (6)$$

and the dispersion relation relating angular frequency,  $\omega = 2\pi f$  and wavenumber:

$$\omega^2 = gk \tanh kH. \quad (7)$$

The factor  $M(f)$  accounts for the decay with depth of the surface wave pressure signal. When  $H < 0.07\lambda$  the shallow water approximation  $\tanh kH \rightarrow kH$  applies, the pressure is hydrostatic, and the wave pressure becomes  $p' = \rho g \eta$ , i.e. independent of depth. When  $H > 0.28\lambda$ ,  $kH > 1.8$  so  $\tanh kH \rightarrow 1$ , the vertical acceleration  $\partial w \partial t$  is non-negligible relative to  $g$ , the deep water approximation applies, and the wave pressure decays exponentially with depth. For peak frequencies of order 0.1 Hz (Fig. 7) and a mean water depth  $\sim 20$  m,  $kH \sim 1$ , so neither the deep nor the shallow water approximation is applicable. Equation 7 was solved at each frequency to obtain  $k$ , and these values of  $k$  were used in Eq. 6 to correct for the decay of wave pressure with depth.

Significant wave height,  $H_s$ , was computed from the variance of the surface elevation via (3)

$$H_s \cong 4\sqrt{m_0}, \quad (8)$$

where  $m_0$  is the integral of the sea surface elevation spectrum,  $S_{\eta\eta}$ , over the wind wave band: taken here to be 0.05 to 0.19 Hz. The upper limit of the band is slightly lower than 0.3 to avoid the noisy region in the spectra.

## 4 Results

### 4.1 Currents

Vertical profiles of speed-bin averaged flow speed are presented in Figs. 5 and 6. These profiles exhibit the vertical structure typical of Grand Passage and other high-flow tidal passages in Nova Scotia (4): i.e. a logarithmic profile consistent with the Law of the Wall extending upward from the bottom to heights of 8 to 10 m. The maximum flow speeds near the surface at the Sig1000 location approached 3 m/s, and were similar in magnitude on both ebb and flood. At the Sig500 location, maximum near surface speeds on ebb were slightly above 2.5 m/s, and much lower on flood, barely reaching 1.5 m/s. These similarities and differences in maximum speeds depending upon the phase of the tide are consistent with the increased pitch and roll variance during rapid water level changes during both flood and ebb at the Sig1000 site (Fig. 4), but only during ebb at the Sig500 location (Fig. 3).

### 4.2 Pressure Spectra

Figure 7 shows the pressure spectra for both instruments for the full experiment, ensemble-averaged in 0.4 m/s signed flow speed intervals. The spectral peaks at  $O(0.1)$  Hz are due to surface gravity waves. At frequencies above the surface wind wave band (0.05 to 0.3), the spectra exhibit relatively “white” (i.e. flat) behaviour: i.e., noise. Unexpectedly, the noise levels are variable, increasing with flow speed in the Signature1000 data during both ebb and flood, but only during ebb in the Signature500 spectra. These dependencies of the pressure noise level on the phase of the tide are further illustrated in Fig. 8, which emphasizes the occurrence of increased noise variance during both flood and ebb tide in the Signature1000 data, but only during ebb tide for the Signature500 (similar to the differences in attitude parameter variability discussed previously in relation to Figs. 3 and 4).

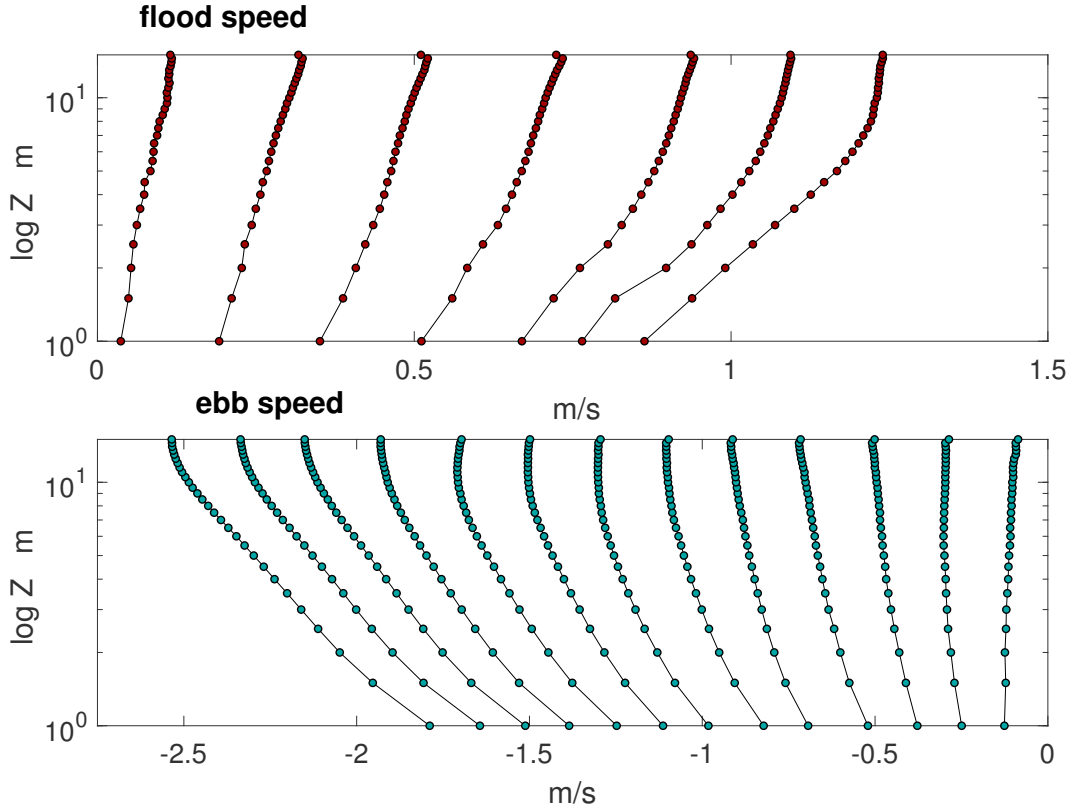


Figure 5: Vertical profiles of mean flow speed recorded with the Signature500, ensemble-averaged over  $0.2 \text{ m s}^{-1}$  intervals based on the speed at 10 m above the instrument. Top panels show profiles during flood, bottom panels during ebb. Panels at left show speed plotted vs.  $z$ ; those at right vs.  $\log z$ .

### 4.3 Significant Wave Height

The values of  $H_s$  estimated from the pressure spectra are shown in Fig. 9. Two episodes with values above 2 m were captured, and it was during these events that large changes in heading occurred (Figs. 3 and 4). Significant wave heights recorded by the Signature1000, which was located inside Grand Passage, were higher than those registered by the Signature500, immediately outside the entrance to the Passage. At times other than those for the two major wave events, the wave height estimates are tidally modulated. This modulation, which is especially evident in the Signature1000 record during ebb tide, is present both during and between the main wave events. Higher wave heights during ebb are expected at the southern entrance to the passage during summertime conditions when the wind direction is typically southwesterly, as wind waves from the Gulf of Maine shoal against the southward-flowing ebb current.

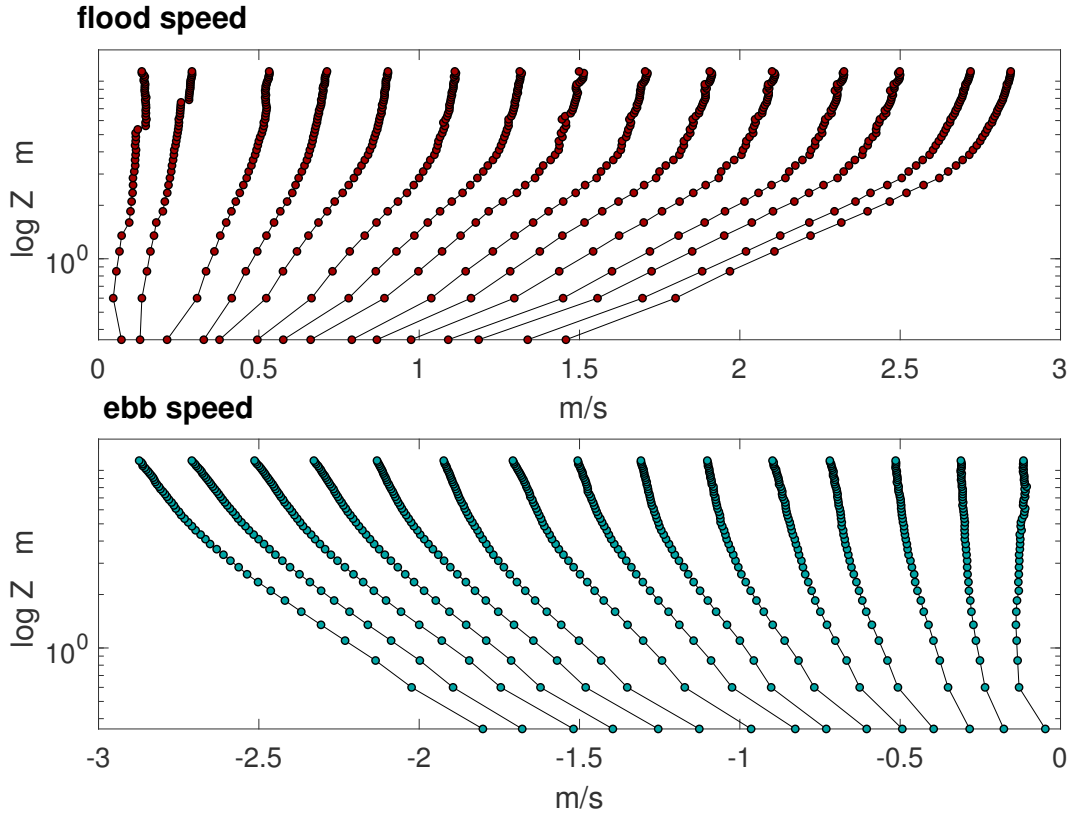


Figure 6: As in Fig. 5, but for the Signature1000. These profiles were computed only for the times when the Sig1000 was not at a high roll angle (see Fig. 4).

#### 4.4 Gimbal mount performance

The time series instrument tilt with respect to vertical – i.e., pitch and roll – in Figs 3 and 4 suggest that the increased variance in these quantities was associated with higher flow speeds. To explore this dependence further, pitch and roll variance are plotted versus mid-depth flow speed in Figure 10. The tilt variances for both instruments exhibit pronounced increases above threshold flow speeds of about 1 m/s for the Signature500, and 1.5 m/s for the Signature1000. Thus, these data indicate that the gimbal mount performed well – in the sense that the ADCPs maintained a stable orientation – for flow speeds up to 1 to 1.5 m/s. This threshold would need to be increased only by a factor of 2 to achieve satisfactory stability for the flow speed conditions in Grand Passage.

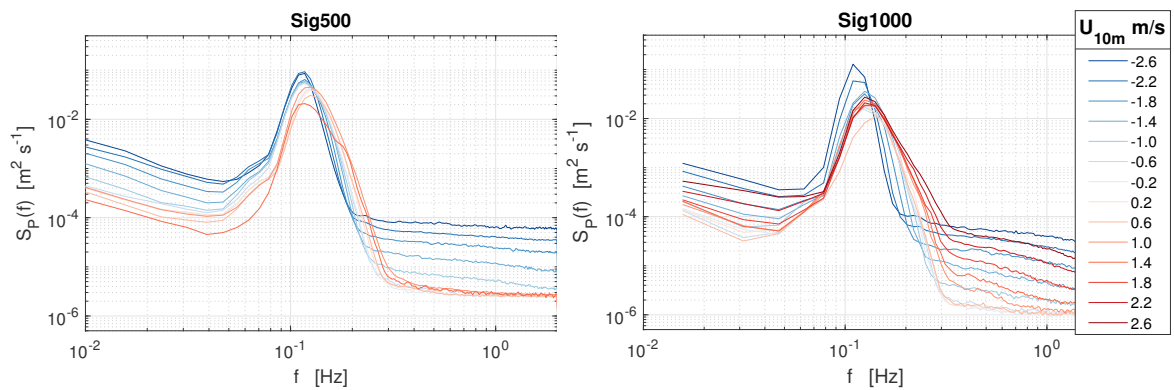


Figure 7: Speedbin-averaged pressure spectra. The signed speed intervals for each speedbin are indicated in the legend. Flood is positive. Note the pronounced peak centred near 0.1 Hz, due to  $O(10)$  s period surface gravity waves. Note also that the noise levels – i.e. the nearly flat spectral levels at frequencies above 0.3 Hz – are flow-speed dependent.

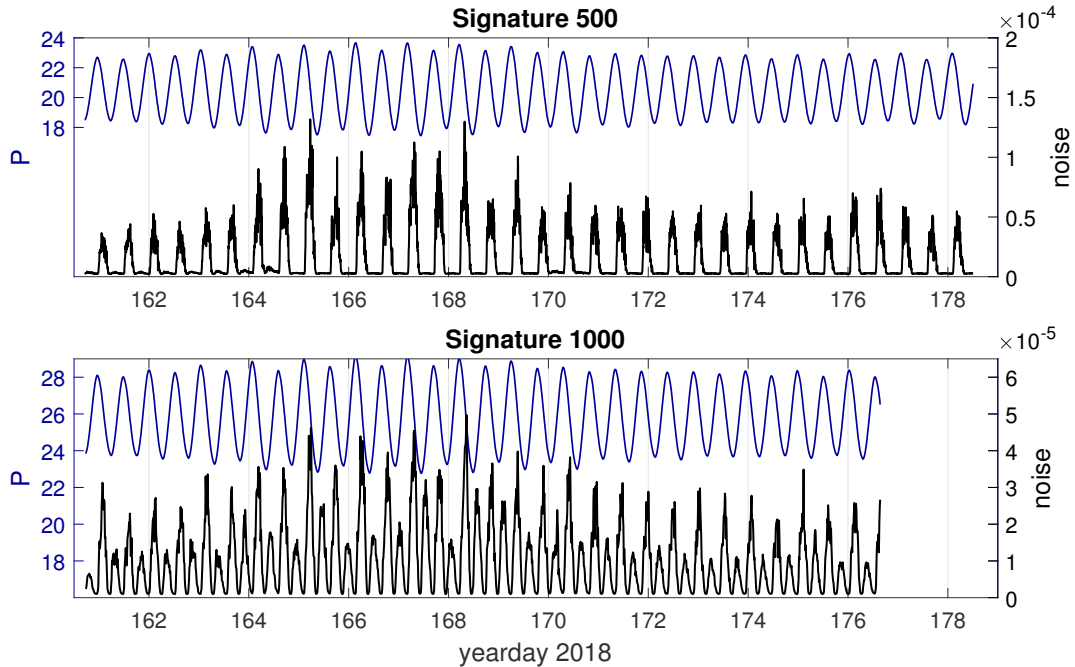


Figure 8: Time series of the noise level in the pressure spectra for both ADCPs, along with the tidal pressure signal. Note the increased noise variance during both flood and ebb in the Signature 1000 data, and during flood only in the Signature500 time series.

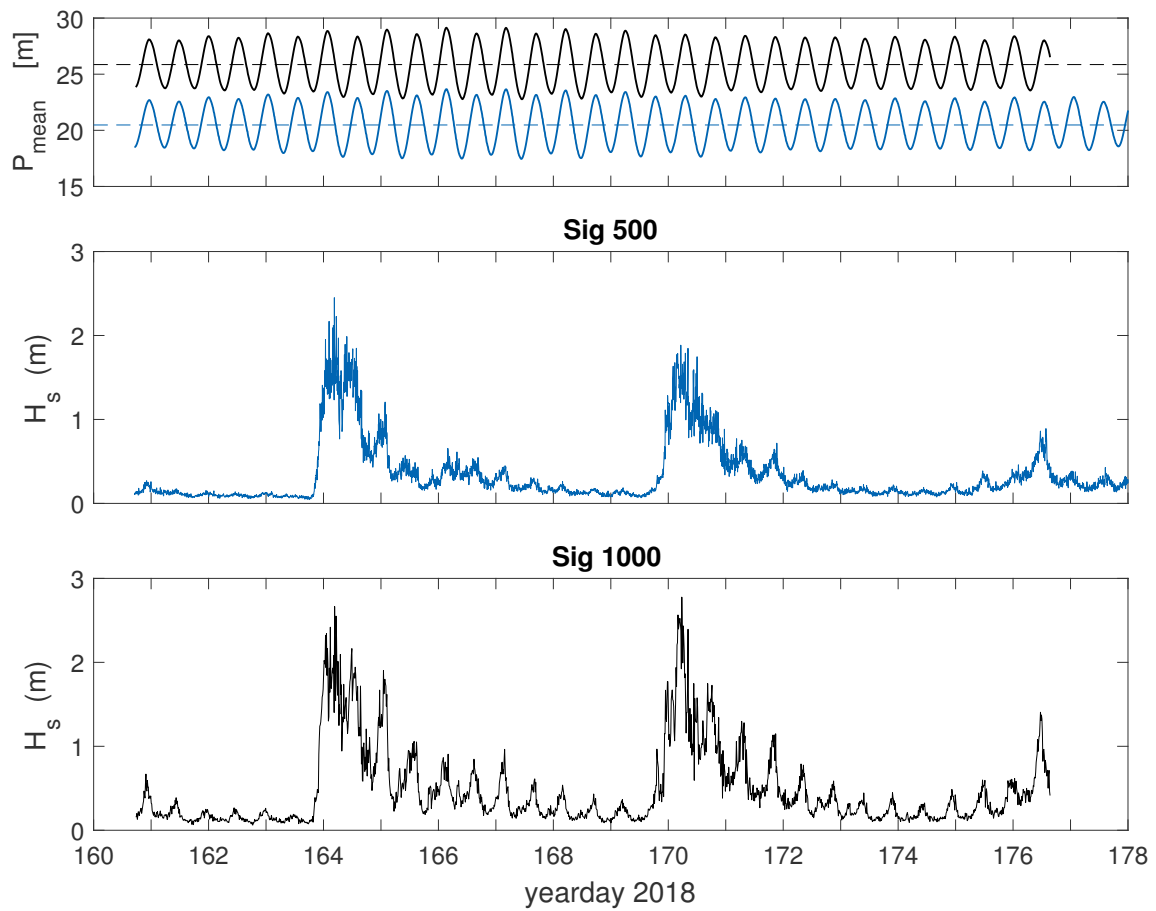


Figure 9: Significant waveheight  $H_s$  computed from the first moments of the pressure spectra, for the Signature500 and the Signature1000.

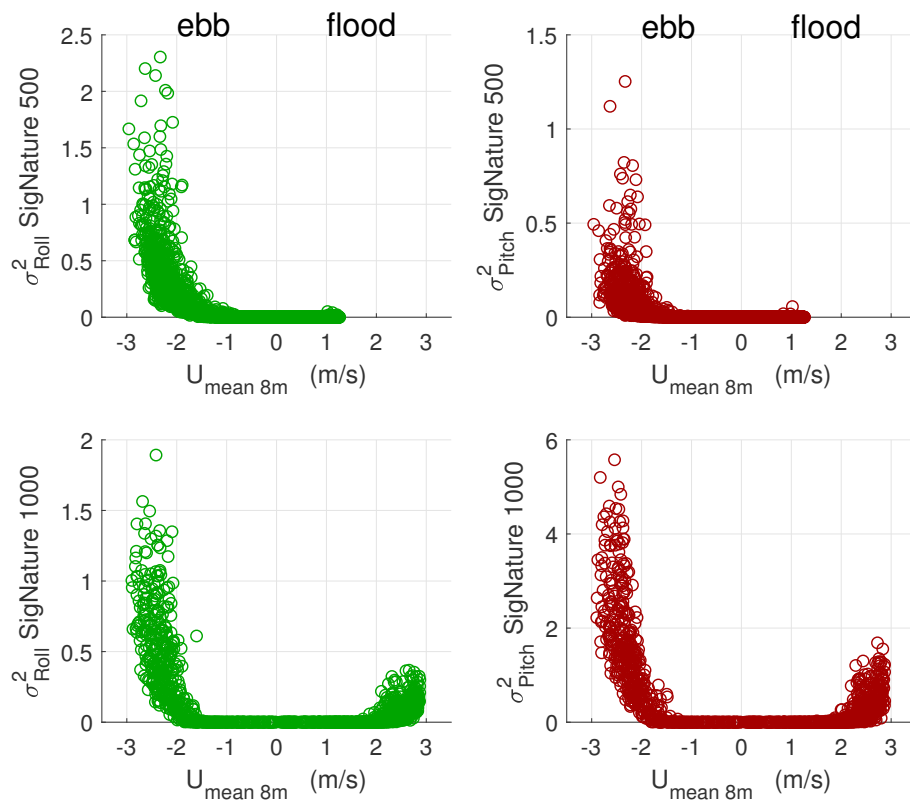


Figure 10: Pitch and roll variance vs mid-depth mean flow speed.

## 4.5 Beam 5 Spectra

As Fig. 10 demonstrates, the both ADCPs maintained a stable orientation for flow speeds less than ca. 1 m/s, possibly opening the door to investigating wave/current/turbulence interactions at ca. 1 m/s flow speeds with this data set. Figures 11 to 14 show the beam5 ensemble-averaged velocity spectra for mean flow speeds between 0.75 and 1 m/s, as a function of height above bottom, for three ranges of significant wave height. The spectra are shown in two forms: one with the noise level included, demonstrating consistency between the observed noise levels and those specified by the manufacturer; the other with this noise level removed, and including a  $-5/3$  slope reference line to indicate the presence of an inertial subrange. All spectra exhibit a peak between 0.1 and 0.2 Hz. The spectral density at the peak increases both with height above bottom, and with significant wave height, unambiguously identifying the peak with surface gravity waves. (Note that, given the water depths at the two ADCP locations, waves at these frequencies are expected to be intermediate to deep-water waves, with orbital velocities increasing toward the surface, consistent with the observed spectra.) The de-noised spectra indicate that the wave peak is superimposed on the  $-5/3$  slope inertial subrange, clearly illustrating the difficulty that the presence of wave motions introduces for estimating turbulent kinetic energy dissipation rates using the spectral method: i.e. it is clear that assumptions have to be made, such as interpolation across the wave peak. The other approach is to implement the structure function method, which involves velocity differences as a function of range, in the expectation that the differencing operation will largely remove the wave velocity. Implementation of the structure function method for these data is part of our ongoing work.

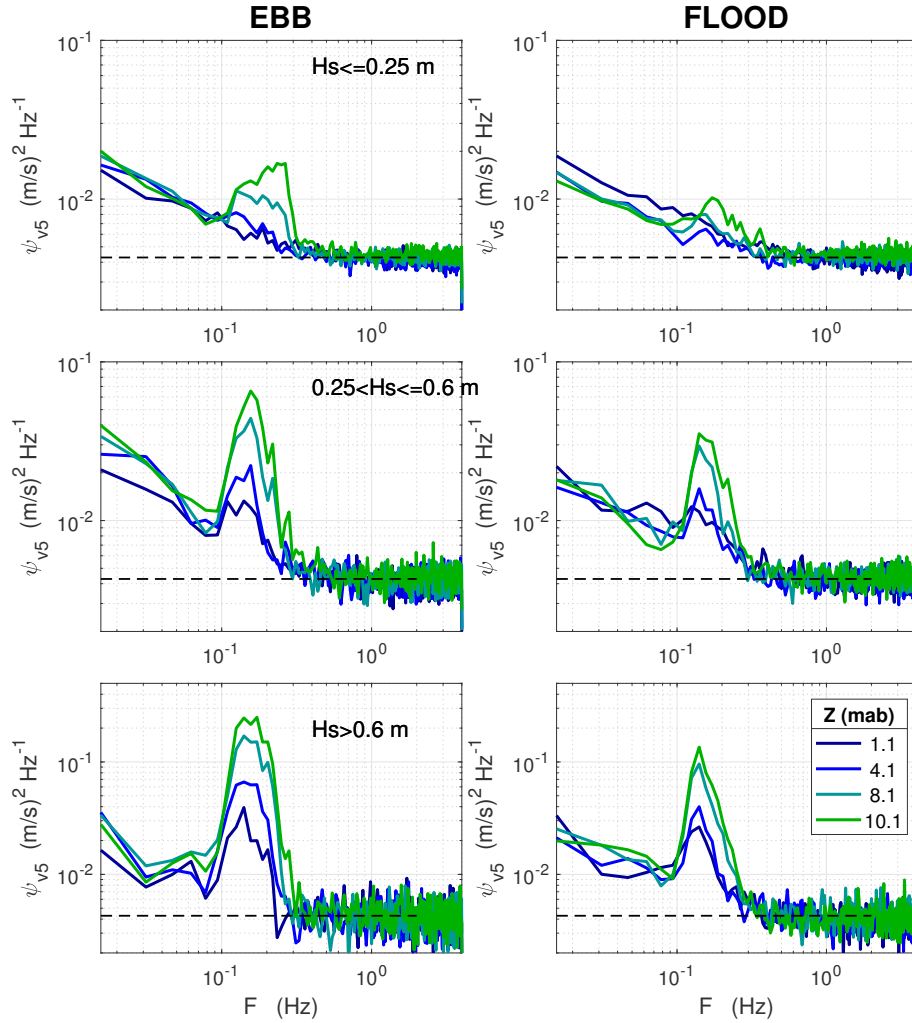


Figure 11: Signature 1000 vertical beam velocity spectra at four selected depth below the surface, for the three wave height ranges and four heights above bottom indicated in the legends, when the mean flow speed was between 0.75 and 1 m/s, separated for ebb/flood conditions. Dashed black lines show the noise level as reported by the manufacturer.

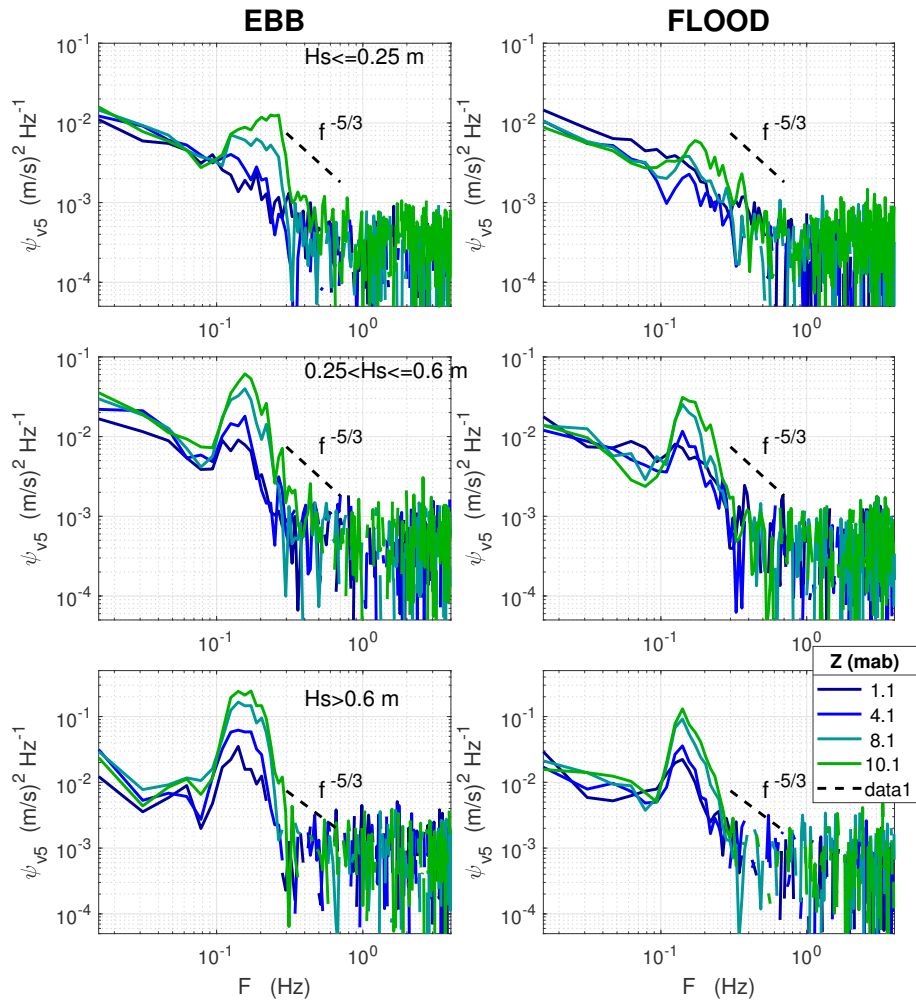


Figure 12: Same as Fig. 11 but with noise spectral density removed. Dashed lines show tangents with an  $f^{-5/3}$  slope.

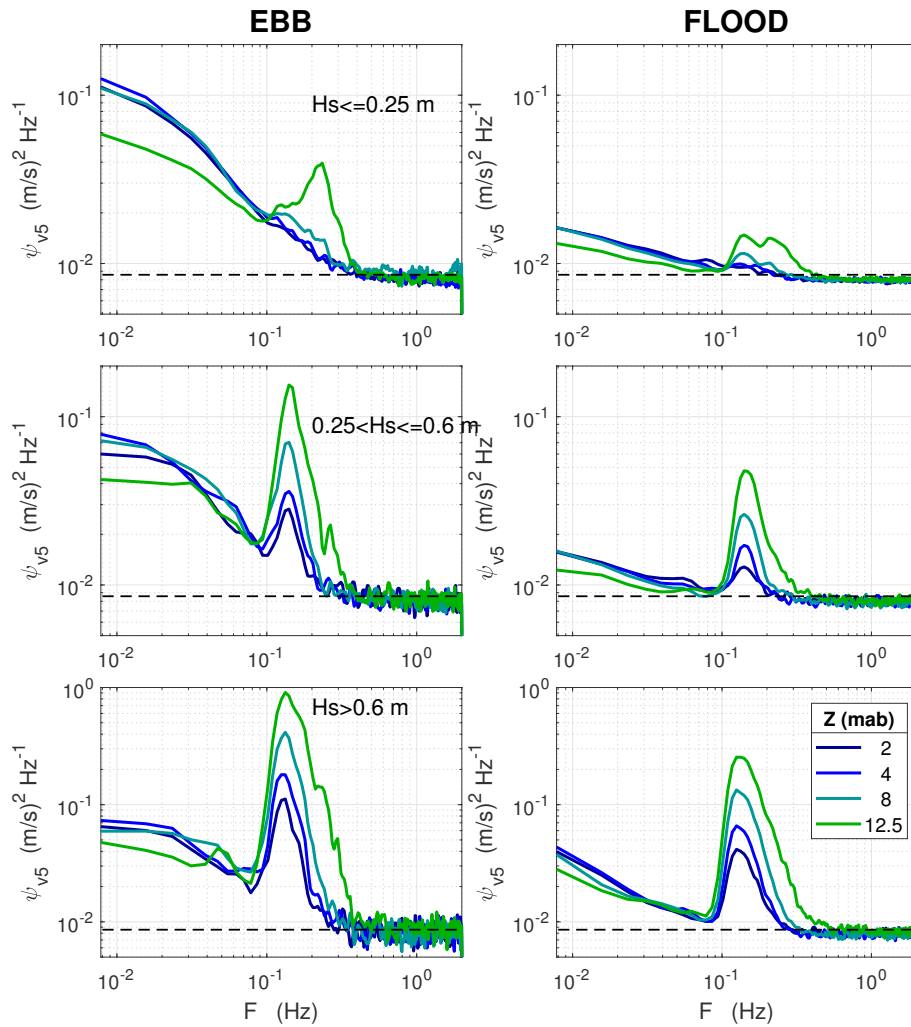


Figure 13: Signature 500 vertical beam velocity spectra at four selected depth below the surface, for the three wave height ranges and four heights above bottom indicated in the legends, when the mean flow speed was between 0.75 and 1 m/s, separated for ebb/flood conditions. Dashed black lines show the noise level as reported by the manufacturer.

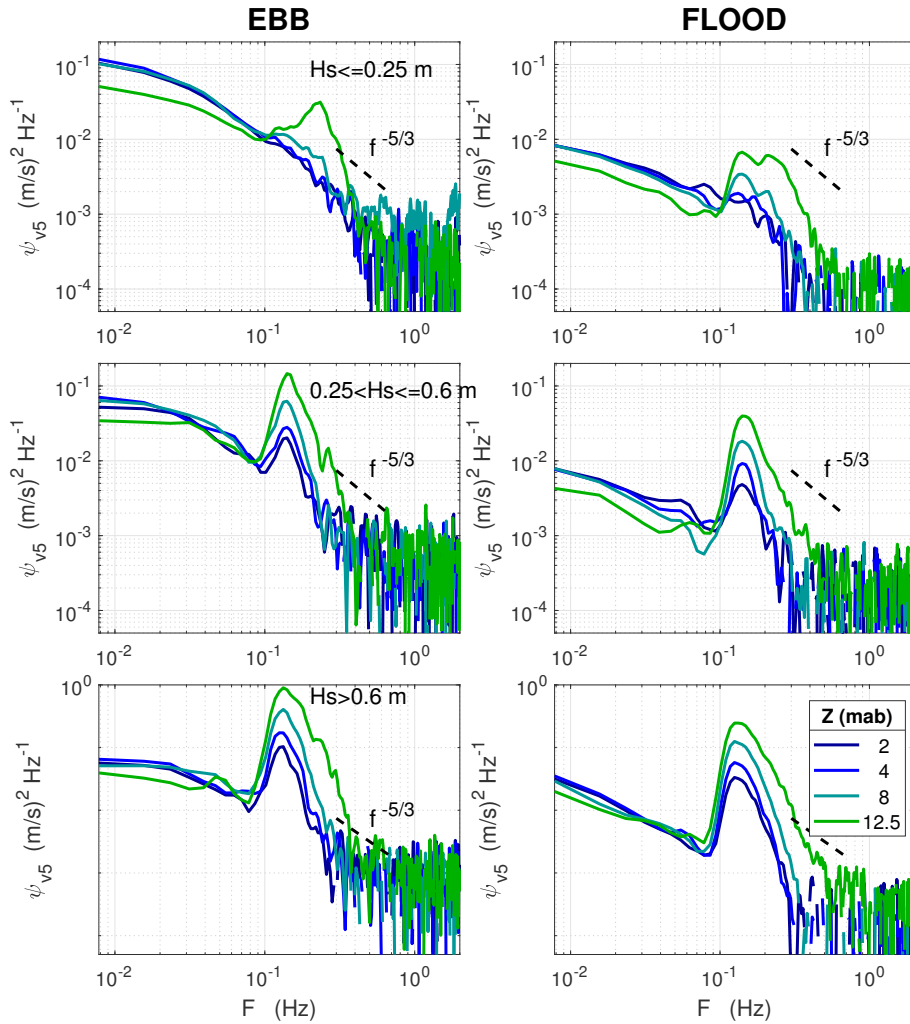


Figure 14: Same as Fig. 13 but with noise spectral density removed. Dashed lines show tangents with an  $f^{-5/3}$  slope.

## 5 Summary and Conclusions

This experiment was less successful than we had hoped. The compressed time schedule, due to the gimbals being delivered a few days prior to deployment, was a factor. In hindsight, instead of pushing ahead with the gimbal installation, we would have been better advised to proceed with our normal fixed-mount procedure for the ADCPs and live with the fact that the ADCPs would not be vertical (because bottom pods would not be level) but would be stable. Doing so would, however, have been a significant deviation from the research plan in the proposal. Regardless, the upshot is that the gimbaled mounts and flow shield adequately stabilized the ADCP orientation only for flow speeds less than ca. 1 m/s. Consequently that the data quality from these deployments was suitable for addressing the wave/current/turbulence interaction question only at these relatively low flow speeds.

Nevertheless, the data do contribute usefully to our quantitative knowledge of wave/current conditions in Grand Passage, since the data on wave conditions in this area are quite sparse (5). The project has also served one of its primary purposes, which was to allow Dr. ten Doeschate to gain experience with acoustic Doppler profiler operation and data processing techniques. The project has had the further benefit that – as of January 2019 – Anneke has joined us as an Ocean Frontier Institute postdoctoral fellow, and in that capacity has continued to work with the June 2018 data as part of the preparation of this Report.

Finally, useful lessons have been learned from this rather hurried trial of a gimbaled mount and flow-shield. Implementing the necessary corrections will require redesign and testing of the bottom-pod frame. In particular, an external battery pack will not be used, eliminating the connecting cable and the resulting torque on the ADCP housing. Also, the increased variance in the ADCP attitude parameters above a threshold mean flow speed indicates that the flow shield was effective only at mid-depth flow speeds below 1 to 1.5 m/s. Improving the flow shield will require a purpose-built welded frame construction and – possibly – an acoustically transparent window over the ADCP transducer assembly.

**Acknowledgements** The authors thank and Mike Huntley and the crew of the *Nova Endeavor*, and Greg Trowse (Luna Oceans), for assistance with the ADCP deployment and recovery operations.

## References

1. J. M. McMillan, *et al.*, *10th European Wave and Tidal Energy Conf.* (Aalborg, Denmark, 2013).
2. P. K. Kundu, *Fluid Mechanics* (Academic Press, San Diego, 1990). 638 pp.
3. E. B. Thornton, R. T. Guza, *J. Geophys. Res.* **88**, 5925 (1983).
4. J. M. McMillan, A. E. Hay, *Journal of Atmospheric and Oceanic Technology* **34**, 5 (2017).
5. C. C. R. Ltd., *Wave and wind climate study - Digby Neck: Final report, Tech. rep.*, Cascadia Coast Research Ltd. (2014).